These data demonstrate that the PHD exerts an MPO-like activity, which induces bacterial death in a chloride-dependent manner. Furthermore, we found that the levels of oxidative damage of ingested bacteria as assessed on the basis of protein carbonylation and lipid peroxidation (*13*) were significantly reduced in the intestines of the *dDuox-RNAi* flies as compared with those seen in the bacteria from control intestines (fig. S7). These results demonstrate that the infection-induced ROS generation by dDuox is responsible for the direct oxidative damage inflicted on ingested microbes.

To demonstrate that the immune susceptibility of *dDuox-RNAi* flies could indeed be attributed to the insufficient enzymatic activity of Duox, we attempted to protect *dDuox-RNAi* flies by reintroducing a variety of Duox enzymes [human Duox (hDuox) 1-2, dDuox, and dDuox-ΔPHD] (Fig. 3A). The reintroduction of both *hDuox* and *dDuox*, but not that of *dDuox-ΔPHD*, markedly augmented the survival rates of the *dDuox-RNAi* flies after natural infection (Fig. 3B). These results are consistent with the previous observations (Fig. 2D), indicating that PHD is required for the microbicidal effects of Duox. The reduced levels of in vitro superoxide-producing activities and of in vivo intestinal ROS in the *dDuox-RNAi* flies were almost completely restored to normal levels by reintroducing the *dDuox* (Fig. 3, C and D). Consistent with this, we detected that microbial persistence within the intestines of the *dDuox-RNAi* flies was reduced to control levels upon reintroduction of *dDuox*, but not upon *dDuox-ΔPHD* expression (Fig. 3E). Taken together, our results demonstrated that intestinal dDuox is responsible for the generation of infection-induced microbicidal ROS and that ROS thus generated are required for limiting the proliferation of local pathogens during gut-microbe interactions.

ROS perform a variety of functions in many biological events, including host defense, development, hormone biosynthesis, fertilization, and diverse intracellular signaling (*2–5*, *14*, *15*, *22–28*). In the present study, we have demonstrated the in vivo role of Duox in innate immunity via mediating epithelial oxidative burst in *Drosophila* gut. Our study broadens the concept of ROS-based immunity by demonstrating that the oxidant-dependent defense system is not restricted to the phagocytes but rather is found in barrier epithelia. In addition to the NF-κB pathway–mediated defense system (*7–11*), the Duox-mediated ROS-dependent defense system involving both gp91^{phox}-like activity and MPO-like activity constitutes another microbicidal arm of *Drosophila* innate immunity. Further delineation of dDuox/IRC-mediated gastrointestinal redox homeostasis will provide important insight into innate immunity and the host-pathogen interaction.

References and Notes

1. R. Medzhitov, C. A. Janeway Jr., *Cell* **91**, 295 (1997).
2. B. M. Babior, *Curr. Opin. Hematol.* **2**, 55 (1995).
3. S. J. Klebanoff, *J. Biol. Chem.* **249**, 3724 (1974).
4. J. M. Pullar, M. C. Vissers, C. C. Winterbourn, *IUBMB Life* **50**, 259 (2000).
5. M. T. Quinn, K. A. Gauss, *J. Leukoc. Biol.* **76**, 760 (2004).
6. H. Rosen, J. R. Crowley, J. W. Heinecke, *J. Biol. Chem.* **277**, 30463 (2002).
7. C. A. Brennan, K. V. Anderson, *Annu. Rev. Immunol.* **22**, 457 (2004).
8. J. A. Hoffmann, J. M. Reichhart, *Nat. Immunol.* **3**, 121 (2002).
9. D. Hultmark, *Curr. Opin. Immunol.* **15**, 12 (2003).
10. B. Lemaitre, *Nat. Rev. Immunol.* **4**, 521 (2004).
11. N. Silverman, T. Maniatis, *Genes Dev.* **15**, 2321 (2001).
12. E. M. Ha *et al.*, *Dev. Cell* **8**, 125 (2005).
13. Materials and methods are available as supporting material on *Science* Online.
14. M. Geiszt, T. L. Leto, *J. Biol. Chem.* **279**, 51715 (2004).
15. J. D. Lambeth, *Nat. Rev. Immunol.* **4**, 181 (2004).
16. G. M. Bokoch, U. G. Knaus, *Trends Biochem. Sci.* **28**, 502 (2003).
17. G. Cheng, Z. Cao, X. Xu, E. G. van Meir, J. D. Lambeth, *Gene* **269**, 131 (2001).
18. M. Geiszt, J. Witta, J. Baffi, K. Lekstrom, T. L. Leto, *FASEB J.* **17**, 1502 (2003).
19. R. A. El Hassani *et al.*, *Am. J. Physiol. Gastrointest. Liver Physiol.* **288**, G933 (2005).
20. R. Forteza, M. Salathe, F. Miot, R. Forteza, G. E. Conner, *Am. J. Respir. Cell Mol. Biol.* **32**, 462 (2005).
21. M. B. Hampton, A. J. Kettle, C. C. Winterbourn, *Blood* **92**, 3007 (1998).
22. J. L. Wong, R. Creton, G. M. Wessel, *Dev. Cell* **7**, 801 (2004).
23. S. G. Rhee, Y. S. Bae, S. R. Lee, J. Kwon, *Sci. STKE* **2000**, pe1 (2000).
24. G. R. Gray *et al.*, *Lancet* **2**, 530 (1973).
25. J. C. Moreno *et al.*, *N. Engl. J. Med.* **347**, 95 (2002).
26. W. A. Edens *et al.*, *J. Cell Biol.* **154**, 879 (2001).
27. X. De Deken *et al.*, *J. Biol. Chem.* **275**, 23227 (2000).
28. C. Dupuy *et al.*, *J. Biol. Chem.* **274**, 37265 (1999).

29. We thank J. Kim for critical comments and F. Miot for human Duox cDNAs. Supported by Korea Science and Engineering Foundation (R2-2002-000-58-0), Center for Cell Signaling Research, and Institut Pasteur Korea. E.-M. H. was supported by the Seoul Science Fellowship.

Supporting Online Material

www.sciencemag.org/cgi/content/full/310/5749/847/DC1
Materials and Methods
SOM Text
Figs. S1 to S7
References

12 July 2005; accepted 5 October 2005
10.1126/science.1117311

Treatment of Autoimmune Neuroinflammation with a Synthetic Tryptophan Metabolite

Michael Platten,[1,3]*† Peggy P. Ho,[1]* Sawsan Youssef,[1] Paulo Fontoura,[1,4] Hideki Garren,[1,5] Eun Mi Hur,[1] Rohit Gupta,[1] Lowen Y. Lee,[1] Brian A. Kidd,[1,6] William H. Robinson,[1,6] Raymond A. Sobel,[2] Michael L. Selley,[7] Lawrence Steinman[1]†

Local catabolism of the amino acid tryptophan (Trp) by indoleamine 2,3-dioxygenase (IDO) is considered an important mechanism of regulating T cell immunity. We show that IDO transcription was increased when myelin-specific T cells were stimulated with tolerogenic altered self-peptides. Catabolites of Trp suppressed proliferation of myelin-specific T cells and inhibited production of proinflammatory T helper–1 (T_H1) cytokines. *N*-(3,4,-Dimethoxycinnamoyl) anthranilic acid (3,4-DAA), an orally active synthetic derivative of the Trp metabolite anthranilic acid, reversed paralysis in mice with experimental autoimmune encephalomyelitis, a model of multiple sclerosis (MS). Trp catabolites and their derivatives offer a new strategy for treating T_H1-mediated autoimmune diseases such as MS.

Degradation of the essential amino acid Trp is now established to play an important role in immunity. The rate-limiting enzyme in Trp catabolism is IDO, and although IDO mRNA is ubiquitously expressed at low levels, IDO protein expression and enzymatic activity are tightly controlled (*1*). During inflammation, IDO is rapidly up-regulated in certain cell types by proinflammatory stimuli and T_H1 cytokines such as interferon-γ (IFN-γ) (*2*). Munn and Mellor first demonstrated a role for Trp catabolism in the control of immune responses in 1998 by showing that inhibition of IDO induces fetal allograft rejection in mice (*3*). Potentially, activated antigen-presenting cells (APCs) catabolize Trp to produce a local immunosuppressive environment able to control T cell homeostasis and self-tolerance during inflammation (*4*, *5*).

In addition to Trp depletion, there is increasing evidence that catabolites of Trp assume an active role in dampening allogenic proliferation and inducing apoptosis of activated T cells (*6*, *7*). These catabolites, collectively referred to as kynurenines (Kyns), are important in the dialogue between the immune system and the central nervous system (CNS) (*8*) and have emerged as an attractive target for drug development (*9*, *10*).

In multiple sclerosis (MS) and its animal model, experimental autoimmune encephalomyelitis (EAE), autoreactive $CD4^+$ T_H1 cells secreting IFN-γ and tumor necrosis factor (TNF) drive inflammation, which is amplified

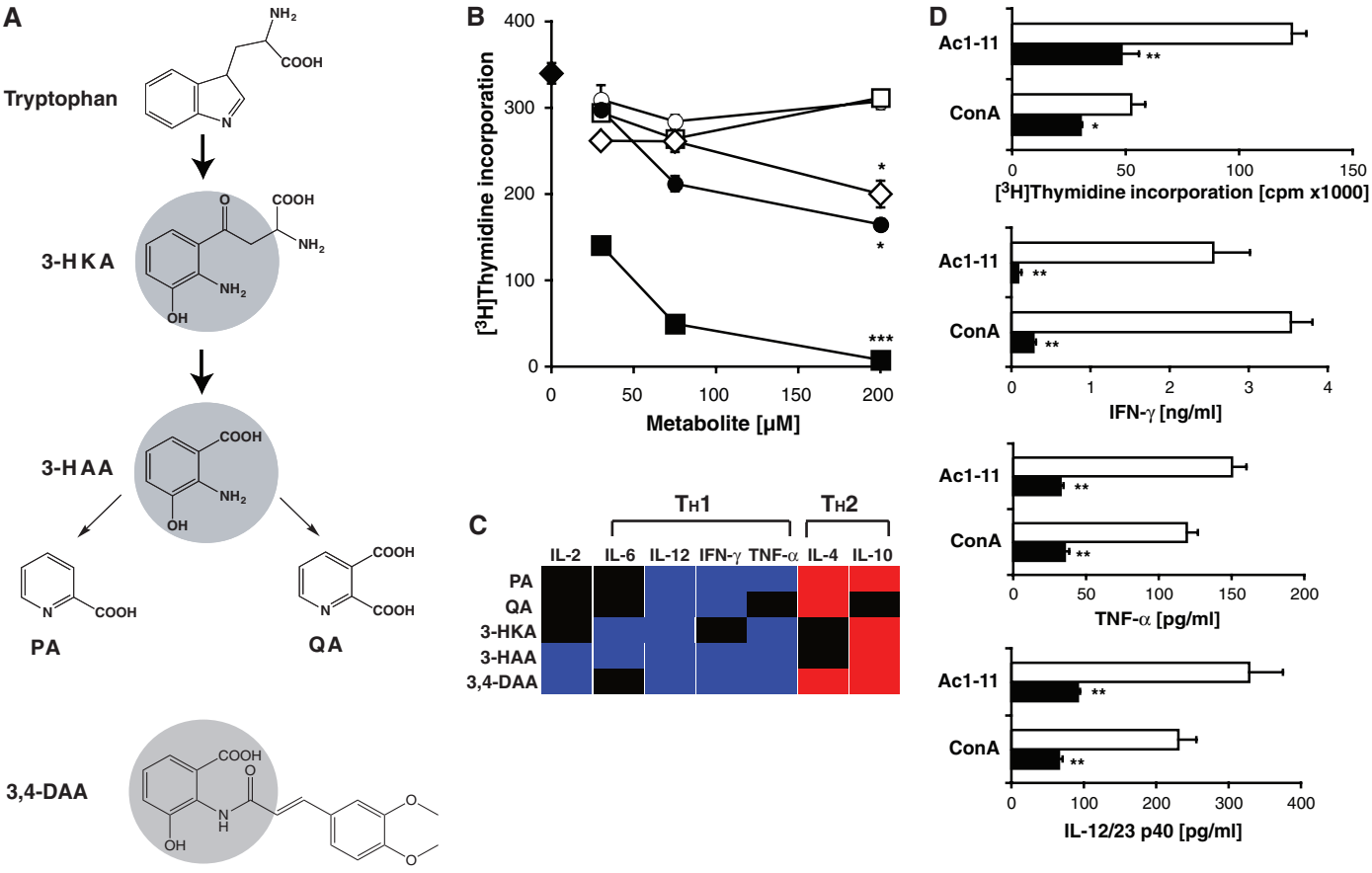

Fig. 1. Modulation of T cell proliferation by Trp metabolites. (**A**) Chemical structure of Trp metabolites. 3-HKA, 3-hydroxykynurenic acid; 3-HAA, 3-hydroxyanthranilic acid; PA, picolinic acid; QA, quinolinic acid; and 3,4-DAA. (**B**) Splenocytes from MBP Ac1-11 TCR transgenic mice were left untreated (control, ◆) or incubated with Trp metabolites PA (○), QA (□), 3-HKA (◇), 3-HAA (●), 3,4-DAA (■) at the concentrations indicated and stimulated with MBP Ac1-11 (5 μg/ml). Splenocytes were pulsed with [^{3}H]thymidine after 48 hours for 18 hours. Data represent mean counts per minute (cpm) and SEM of triplicates and are representative of four independent experiments. *$P < 0.05$, ***$P < 0.001$. (**C**) Splenocytes from MBPAc1-11 TCR transgenic mice were activated with MBP Ac1-11 (0.5 to 2.5 μg/ml) in the absence or presence of Trp metabolites PA, QA, 3-HKA, 3-HAA, or 3,4-DAA at 200 μM (IL-2, IFN-γ, TNF-α, IL-6, and IL-12/23 p40) or 30 μM (IL-4, IL-10). Cytokine release was measured after 48 hours (IL-2, IL-6, IL-12/23 p40), 72 hours (IFN-γ, TNF-α), or 120 hours (IL-4, IL-10) by using enzyme-linked immunosorbent assay (ELISA, OptEIA Cytokine Sets, BD Pharmingen). Data are displayed as a heat map. Raw data are presented in table S2. (**D**) MBP Ac1-11 TCR transgenic mice ($n = 3$ per group) were fed with 3,4-DAA for 5 days (500 mg/kg per day). Pooled splenocytes of vehicle (Na-CMC)–treated (white bars) or 3,4-DAA–treated (filled bars) mice were stimulated with MBP Ac1-11 (5 μg/ml) or concanavalin A (ConA) (2 μg/ml) in vitro. Proliferation and cytokine analysis were performed as described. Mean values and SEM of triplicates are given, and data are representative of two independent experiments. *$P < 0.05$, **$P < 0.01$.

within the CNS by microglia (*11*–*13*). Experimental therapeutic approaches aimed at skewing the cytokine profile of myelin-specific T_H cells from T_H1 to T_H2 have included altered peptide ligands (APLs) (*14*, *15*), hydroxymethylglutaryl coenzyme A (HMG-CoA) reductase inhibitors ("statins"), and DNA vaccination combined with gene delivery of interleukin 4 (IL-4) (*16*–*18*). APLs are peptides modified at crucial receptor binding residues to modulate proliferation and the cytokine profile of antigen-specific T cells by altering the strength of T cell receptor (TCR) signaling (*14*). Deviation of cytokine responses toward T_H2 is also a mechanism of action of glatiramer acetate, an example of an APL, which is an approved treatment for multiple sclerosis (*19*, *20*). Consequently, APLs inducing a T_H2 immune response have emerged as a potential therapeutic strategy to induce self-tolerance to autoantigens and to treat autoimmune diseases such as MS (*21*–*24*). Such approaches aimed at inducing a T_H2 shift have been relatively promising in reversing ongoing paralytic disease in the EAE model.

Initially, we aimed at identifying gene transcripts that are differentially regulated in T cells treated with APL. To do this, a T cell line generated from mice with a transgenic TCR specific for the myelin basic protein (MBP) peptide Ac1-11 was used for a gene microarray analysis (*25*). The APL MBP Ac1-11[4Y] binds to the major histocompatibility complex (MHC) class II I-A^u with greater affinity than the native peptide. MBP Ac1-11 induces primarily a T_H1 response, whereas MBP Ac1-11[4Y] promotes a T_H2 response (*26*). Transcripts encoding IDO were more than 70-fold up-regulated after 48 hours in MBP Ac1-11[4Y]–activated T cells compared with MBP Ac1-11–activated cells (*27*) (table S1). These data suggested a direct role of IDO in the tolerogenic effects of APLs.

We next tested the hypothesis that Trp metabolites (Kyns), generated by the enzymatic activity of IDO, play a role in regulating activation of myelin-specific T cells (*25*). Splenocytes isolated from MBP Ac1-11 TCR transgenic B10.PL mice were stimulated with

[1]Department of Neurology and Neurological Sciences, Beckman Center for Molecular Medicine, [2]Department of Pathology (Neuropathology), Stanford University, Stanford, CA 94305, USA. [3]Department of General Neurology and Hertie-Institute for Clinical Brain Research, University of Tübingen, 72076 Tübingen, Germany. [4]Department of Immunology, Faculty of Medical Sciences, New University of Lisbon, 1169–056 Lisbon, Portugal. [5]Bayhill Therapeutics Inc., Palo Alto, CA 94303, USA. [6]Geriatrics Research and Education Clinical Center (GRECC), Veterans Affairs Health System, Palo Alto, CA 94304, USA. [7]Angiogen Pharmaceuticals Pty. Ltd., Sydney, NSW 2000, Australia.

*These authors contributed equally to this work.
†To whom correspondence should be addressed. E-mail: steinman@stanford.edu (L.S.), michael.platten@uni-tuebingen.de (M.P.)

MBP Ac1-11 in combination with the Trp metabolites picolinic acid (PA), quinolinic acid (QA), 3-hydroxyanthranilic acid (3-HAA), 3-hydroxykynurenic acid (3-HKA), and the synthetic derivative 3,4-DAA (*25*). 3,4-DAA was selected because it shares the anthranilic acid core with 3-HKA and 3-HAA (Fig. 1A) and because it is an orally active compound with favorable pharmacokinetics in humans (*28*). 3-HAA, 3-HKA, and 3,4-DAA suppressed antigen-specific proliferation of MBP Ac1-11 TCR transgenic $CD4^+$ T cells (Fig. 1B). Suppression of T cell response by 3,4-DAA was associated with a G_1/S-phase arrest in $CD4^+$ T cells rather than cytotoxic effects (fig. S1). Both natural Trp metabolites and 3,4-DAA reduced the release of IL-2, IFN-γ, and TNF-α from MBP Ac1-11 TCR transgenic T cells after antigen stimulation. Conversely, IL-4 and IL-10 were increased (Fig. 1C; table S2). Thus, both natural Trp metabolites and 3,4-DAA skew the cytokine profile of these T cells from T_H1 to T_H2.

To examine the effects of 3,4-DAA on myelin-specific T cells in vivo, MBP Ac1-11 TCR transgenic mice were fed with 3,4-DAA for 5 days (*25*) (supporting online text, note S1). Splenocytes isolated from these animals showed reduced MBP Ac1-11–specific proliferation. Similarly, antigen-induced release of IFN-γ, TNF-α, and IL-12/23 p40 was profoundly suppressed (Fig. 1D), which indicates that 3,4-DAA is active when given orally to suppress the activation of autoreactive T_H1 cells.

Adaptive immunity in $CD4^+$ T_H cells requires antigen presentation on MHC class II molecules and delivery of costimulatory signals via molecules such as CD40, CD80, and CD86, all inducible by IFN-γ (*29*). To assess the influence of Trp metabolites on antigen presentation, we used EOC20 microglial cells as a model (*25*). EOC20 cells express MHC class II and costimulatory molecules constitutively at low levels, and these cells rapidly upregulate on exposure to IFN-γ. 3,4-DAA decreased IFN-γ–induced cell surface expression of MHC class II and costimulatory molecules (Fig. 2A) (*30*). 3,4-DAA–mediated suppression of IFN-γ–induced MHC class II expression in EOC20 cells was paralleled by an inhibition of the MHC class II transactivator (CIITA) (Fig. 2B). In addition, 3,4-DAA suppressed expression of inducible nitric oxide synthase (iNOS) and nitric oxide (NO) release from EOC20 cells induced by IFN-γ and lipopolysaccharide (LPS) (Fig. 2, C and D). On the basis of these results, we hypothesized that 3,4-DAA might interfere with IFN-γ signaling: Type I and type II interferons predominantly signal through phosphorylation of signal transducer and activator of transcription (STAT) 1α (*31*); and consistent with the previous results, phosphorylation of STAT1α induced by IFN-γ was suppressed after incubation with 3,4-DAA (Fig. 2E). 3,4-DAA also suppressed the activation of APCs in vivo (fig. S3, table S3).

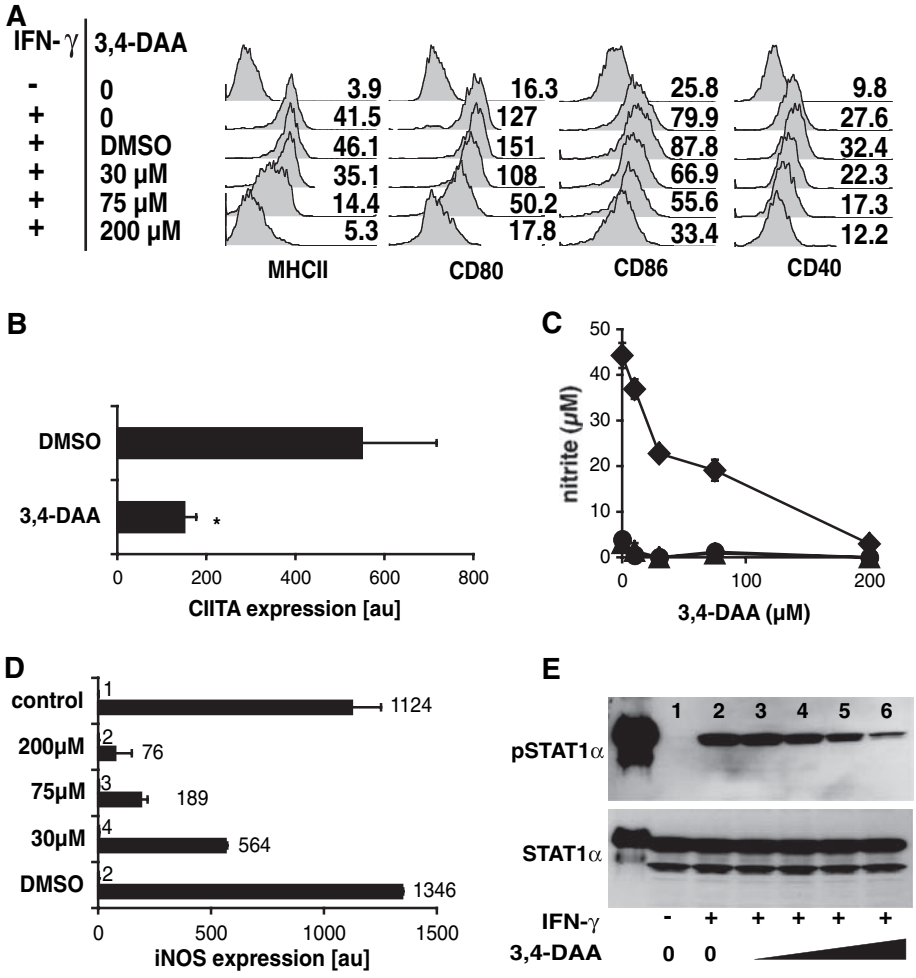

Fig. 2. Mechanisms of APC function modulated by 3,4-DAA. EOC20 cells were incubated with medium alone, dimethyl sulfoxide vehicle (DMSO), or 3,4-DAA at the concentrations indicated and were stimulated with IFN-γ (200 U/ml) and/or LPS (200 ng/ml). (**A**) Cell surface expression of MHC class II ($I\text{-}A^k$), CD40, CD80, and CD86 was determined after 48 hours using flow cytometry. Histograms are representative of three independent experiments. Values represent mean fluorescent indices. (**B**) RNA was extracted after 24 hours and reverse-transcribed. CIITA cDNA expression was quantified by using real-time polymerase chain reaction (PCR). Values represent mean arbitrary expression levels of triplicates and SEM normalized to expression of β-actin. Data are representative of two independent experiments. $*P < 0.05$. (**C**) Nitrite release of unstimulated (▲), IFN-γ–stimulated (●), or IFN-γ– and LPS-stimulated cells (◆) was determined after 48 hours by using the Griess assay. Values are mean nitrite concentration and SEM of triplicates and are representative of three independent experiments. (**D**) RNA was extracted after 24 hours and reverse-transcribed. iNOS cDNA expression was semiquantified by using PCR in real time. Values of unstimulated (white bars) and IFN-γ–stimulated (black bars) represent mean arbitrary expression levels of triplicates and SEM normalized to expression of β-actin. Data are representative of two independent experiments. (**E**) Western blot analysis of whole-cell protein extracted 15 min after stimulation with IFN-γ by using a phospho-specific STAT1α antibody. The membrane was reprobed with a non–phospho-specific STAT1α antibody to ensure equal loading.

To assess whether 3,4-DAA suppresses the function of autoreactive T_H1 cells, we tested the compound in vivo using the relapsing-remitting version of EAE, which serves as a model of relapsing-remitting MS (*25*). As patients with relapsing-remitting MS are typically treated after the first onset of clinical symptoms to prevent further attacks, we initiated treatment after the onset of disease. Although vehicle-treated animals displayed severe relapses throughout the course of disease, animals treated with 3,4-DAA had fewer and milder relapses and less severe disease (Fig. 3A). At multiple dose levels, there was significant reduction in clinical disease index (CDI) and peak relapse score (table S4).

Concordant with the capacity of 3,4-DAA to suppress activation of myelin-specific T_H1 cells in vitro, the frequency of activated T cells was decreased in mice treated with 3,4-DAA (Fig. 3B). Moreover, PLP-specific T cell proliferation and the release of IFN-γ, TNF-α,

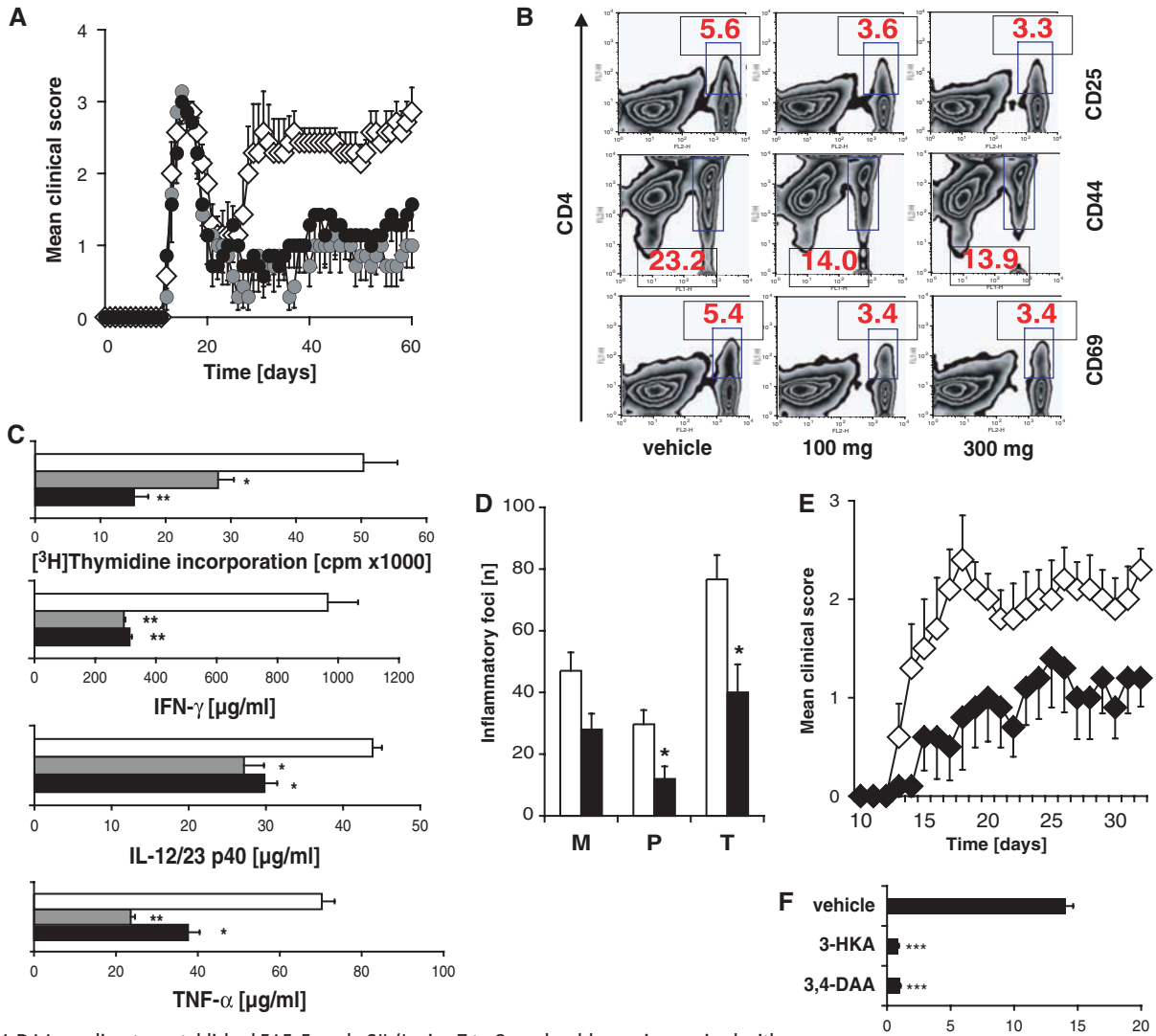

Fig. 3. 3,4-DAA ameliorates established EAE. Female SJL/J mice 7 to 8 weeks old were immunized with PLP p139-151. Treatment was initiated at the peak of clinical symptoms (day 16 to day 18) by oral gavage twice daily (3,4-DAA) or by intraperitoneal injections once daily (3-HKA). (**A**) Clinical scores of vehicle-treated mice (◇) and mice treated with 3,4-DAA at 100 mg/kg per day (●) or 300 mg/kg per day (●) (0, asymptomatic; 1, limp tail; 2, partial hind limb paresis; 3, hind limb paralysis; 4, quadriplegia; 5, moribund or dead) were assessed each day. Data represent mean scores (n = 9, vehicle and 300 mg/kg per day; n = 10, 100 mg/kg per day) and SEM. (**B**) Flow cytometric analysis of pooled splenocytes of vehicle-treated (n = 6) or 3,4-DAA–treated (n = 7, 100 mg/kg per day; n = 6, 300 mg/kg per day) mice isolated 60 days post immunizations. Values represent double-positive cells, that is, $CD4^+$ and $CD69^+$, $CD44^+$, or $CD25^+$. (**C**) Pooled splenocytes of vehicle-treated (n = 6, white bars), or 3,4-DAA–treated (n = 7, 100 mg/kg per day, gray bars; n = 6, 300 mg/kg per day, black bars) were isolated after 60 days and stimulated in vitro with PLP p139-151 (20 μg/ml). Proliferation was assessed as in Fig. 1B, except cells were pulsed after 72 hours of culture. Cytokines were analyzed as in Fig. 1C. Data represent mean values of triplicates and SEM. $*P < 0.05$, $**P < 0.01$. (**D**) Brains and spinal cords were extracted 60 days after immunization. Infiltration of inflammatory cells was counted in randomly chosen brains from vehicle-treated (n = 3, white bars) and 3,4-DAA–treated (n = 3, 100 mg/kg per day, black bars) by a neuropathologist blinded to the treatment. M, meningeal foci; P, parenchymal foci; T, total number of foci. Data represent mean number of inflammatory foci and SEM. $*P < 0.05$. (**E**) Lymph node cells from mice with EAE that had been treated with vehicle (◇) or 3,4-DAA (200 mg/kg per day, ◆) were stimulated in vitro with PLP p139-151 (10 μg/ml) and adoptively transferred into SJL/J recipient mice that had been immunized 8 days before adoptive transfer with PLP p139-151. Data represent mean clinical scores. (**F**) Lymph node cells from mice with EAE that had been treated with vehicle, 3,4-DAA (200 μg/kg per day), or 3-HKA (150 mg/kg per day) were stimulated in vitro with PLP p139−151 (10 μg/ml). Cytokines were analyzed as in Fig. 3C. Values are displayed as amounts of cytokines released by cells stimulated with PLP p139-151 divided by amounts of cytokines released by unstimulated cells. Data represent mean values and SEM. $**P < 0.01$, $***P < 0.001$.

and IL-12/23 p40 were decreased after treatment with 3,4-DAA (Fig. 3C) (SOM text, note S2). Next, assessment of brains and spinal cords of mice with EAE revealed a reduction of parenchymal and total inflammatory foci in CNS tissue from mice treated with 3,4-DAA compared to vehicle-treated mice (Fig. 3D).

We evaluated whether activation of APCs in the CNS was suppressed in vivo (*25*, *32*). Consistent with previous results, expression of MHC class II, CD40, CD80, CD86, and iNOS was drastically reduced in spinal cord microglial cells when mice with EAE had been treated with 3,4-DAA (Fig. 4A). Moreover, the expression of the CIITA, iNOS, TNF-α, and IL-12/23 p40 genes was reduced in spinal cords of animals treated with 3,4-DAA (Fig. 4B). Taken together, these results indicate suppression of APCs as a key mechanism underlying the immunosuppressive effects of 3,4-DAA.

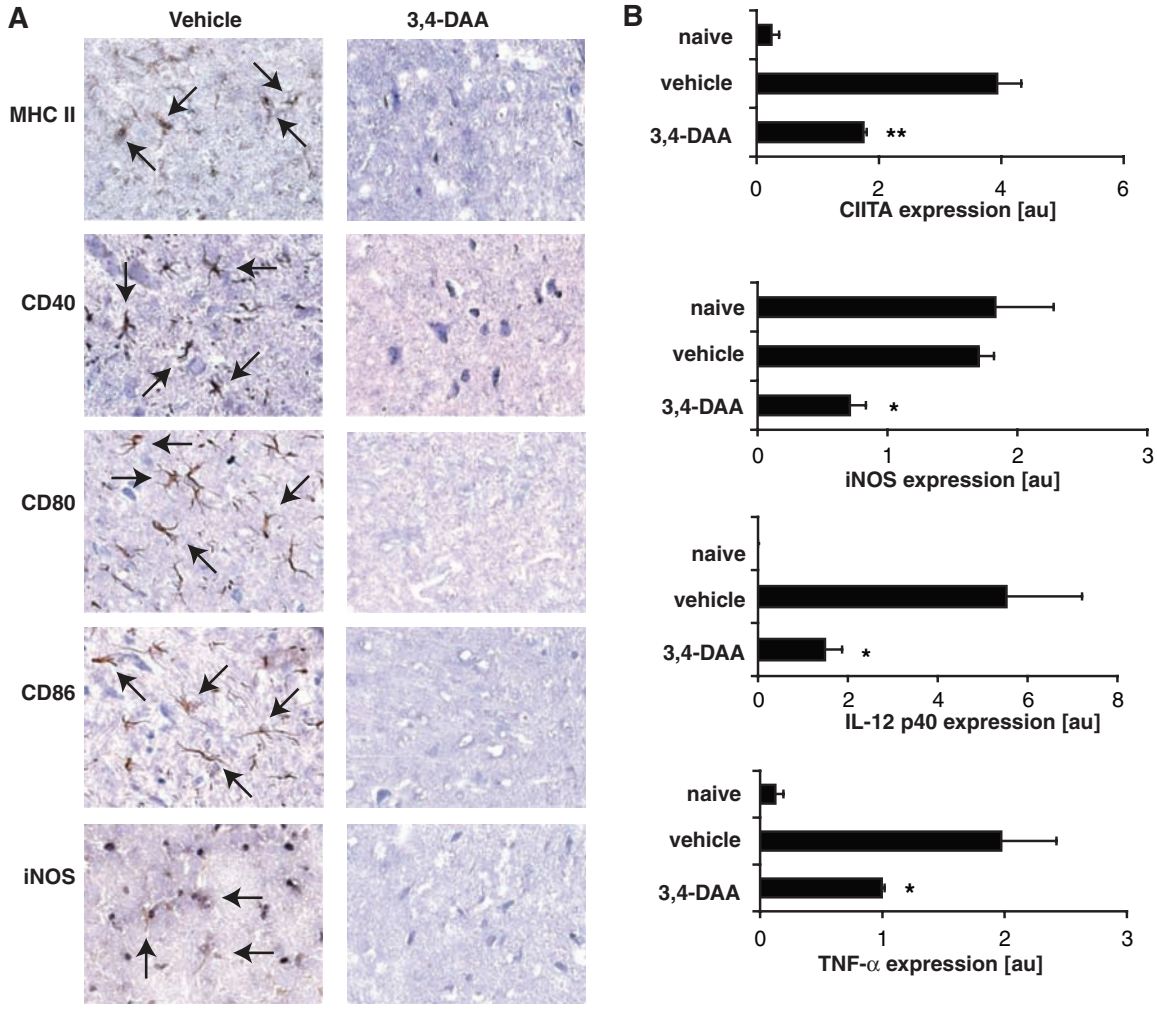

Fig. 4. 3,4-DAA suppresses the activation of CNS antigen-presenting cells in EAE. (**A**) Female SJL/J mice 7 to 8 weeks old were immunized with PLP p139-151 two days after the initiation of treatment with 3,4-DAA (200 mg/kg per day) by oral gavage twice daily. 12 days after immunization, brains and spinal cords were removed and stained for MHC class II ($I\text{-}A^k$), CD40, CD80, CD86, and iNOS. (**B**) Female SJL/J mice 7 to 8 weeks old were immunized with PLP p139-151. Treatment with 3,4-DAA was initiated at day 16. Naïve animals served as a control. RNA was isolated from spinal cords 60 days after immunization ($n = 3$). After reverse transcription, cDNA expression of the indicated transcripts was analyzed by using real-time PCR. Values represent mean arbitrary expression levels of triplicates and SEM normalized to expression of β-actin. Data are representative of three independent experiments. $^*P < 0.05$, $^{**}P < 0.01$.

We finally assessed whether suppression of myelin specific T_H1 cells results from direct inhibition of these cells by 3,4-DAA, or whether this suppression might be mediated by myelin-specific T_H2-like cells induced by treatment with the drug (*25*). Myelin-reactive lymph node cells from donor mice treated with 3,4-DAA after onset of EAE delayed the onset and ameliorated the symptoms of EAE when adoptively transferred into recipient mice that had been immunized with PLP p139-151 (Fig. 3E). Finally, administration of either the natural Trp metabolite 3-HKA or the synthetic Trp metabolite 3,4-DAA to SJL mice with EAE induced release of IL-10 from PLP p139-151–reactive lymph node cells (Fig. 3F) (*25*). Induction of IL-10 with these compounds in myelin-specific T cells was also observed in vitro (Fig. 1C). Collectively, these data indicate that natural Trp metabolites induce antigen-specific IL-10–producing T cells with regulatory potential in vitro and in vivo. Moreover, these findings strongly suggest that 3,4-DAA, structurally related to Trp metabolites, has similar physiologic effects as well.

Interestingly, the structurally related immune regulators, linomide and laquinimod with a yet unidentified mechanism of action, are quinoline carboxamides with structural homology to these same Trp metabolites (fig. S5). Both linomide and laquinimod are effective in treating EAE and show some efficacy in patients with MS (*33*, *34*). Quinoline carboxamides, however, are cardiotoxic. Thus, trials of linomide in patients with MS have been halted. These observations further support our findings that Trp metabolites may represent a novel class of drugs effective in treating T_H1-mediated autoimmune diseases. Our results indicate that 3,4-DAA, by acting as a mimetic of the Trp catabolites, can replace the physiologic role of natural Trp catabolites in inhibiting autoreactive T_H1 cells. Orally active derivatives of Trp metabolites, such as 3,4-DAA, may thus represent a new class of drugs for therapy to treat ongoing T_H1-mediated autoimmune diseases.

References and Notes

1. A. L. Mellor, D. H. Munn, *Nat. Rev. Immunol.* **4**, 762 (2004).
2. M. W. Taylor, G. S. Feng, *FASEB J.* **5**, 2516 (1991).
3. D. H. Munn *et al.*, *Science* **281**, 1191 (1998).
4. U. Grohmann, F. Fallarino, P. Puccetti, *Trends Immunol.* **24**, 242 (2003).
5. D. H. Munn, A. L. Mellor, *Trends Mol. Med.* **10**, 15 (2004).
6. G. Frumento *et al.*, *J. Exp. Med.* **196**, 459 (2002).
7. P. Terness *et al.*, *J. Exp. Med.* **196**, 447 (2002).
8. L. Steinman, *Nat. Immunol.* **5**, 575 (2004).
9. R. Schwarcz, *Curr. Opin. Pharmacol.* **4**, 12 (2004).
10. T. W. Stone, L. G. Darlington, *Nat. Rev. Drug Discov.* **1**, 609 (2002).
11. L. Steinman, *Nat. Immunol.* **2**, 762 (2001).
12. M. J. Carson, *Glia* **40**, 218 (2002).
13. M. Platten, L. Steinman, *Nat. Med.* **11**, 252 (2005).
14. B. D. Evavold, J. Sloan-Lancaster, P. M. Allen, *Immunol. Today* **14**, 602 (1993).
15. L. B. Nicholson, J. M. Greer, R. A. Sobel, M. B. Lees, V. K. Kuchroo, *Immunity* **3**, 397 (1995).
16. S. Brocke *et al.*, *Nature* **379**, 343 (1996).
17. H. Garren *et al.*, *Immunity* **15**, 15 (2001).
18. S. Youssef *et al.*, *Nature* **420**, 78 (2002).
19. P. W. Duda, M. C. Schmied, S. L. Cook, J. I. Krieger, D. A. Hafler, *J. Clin. Invest.* **105**, 967 (2000).
20. L. Steinman, *Science* **305**, 212 (2004).
21. B. Bielekova *et al.*, *Nat. Med.* **6**, 1167 (2000).
22. C. P. Genain, S. S. Zamvil, *Nat. Med.* **6**, 1098 (2000).
23. L. Kappos *et al.*, *Nat. Med.* **6**, 1176 (2000).
24. M. Feldmann, L. Steinman, *Nature* **435**, 612 (2005).
25. Materials and methods are available as supporting material on *Science* Online.
26. C. I. Pearson, W. van Ewijk, H. O. McDevitt, *J. Exp. Med.* **185**, 583 (1997).
27. Data were submitted to the Gene Expression Omnibus (GEO) and can be accessed at www.ncbi.nlm.nih.gov/geo with accession number GSE3401.
28. M. Isaji, H. Miyata, Y. Ajisawa, *Cardiovasc. Drug Rev.* **16**(3), 288 (1998).
29. B. M. Carreno, M. Collins, *Annu. Rev. Immunol.* **20**, 29 (2002).
30. 3,4-DAA did not reduce cell viability at concentrations up to 200 μM as assessed by propidium iodine staining (fig. S2).

31. D. S. Aaronson, C. M. Horvath, *Science* **296**, 1653 (2002).
32. Treatment with 3,4-DAA was associated with a markedly suppressed lymphocytic infiltration in the spinal cords of mice with EAE (fig. S4).
33. I. L. Tan, G. J. Lycklama a Nijeholt, C. H. Polman, H. J. Ader, F. Barkhof, *Mult. Scler.* **6**, 99 (2000).
34. C. Polman *et al.*, *Neurology* **64**, 987 (2005).
35. This work was supported by grants from the NIH, the National MS Society, the Phil N. Allen Trust to L.S., and funding from Angiogen Pharmaceuticals Pty. Ltd. M.P. is a recipient of an Emmy-Noether-Fellowship from the German Research Foundation (Deutsche Forschungsgemeinschaft, DFG PL 315/1-1). M.S. is a major stockholder of Angiogen Pharmaceuticals Pty. Ltd., which develops and commercializes new therapies in inflammation, neurological disease, and cancer. We thank M. J. Eaton and M. Britschgi for excellent technical assistance. K. Yokoyama and H. McDevitt kindly provided the MBP Ac1-11 TCR transgenic mice used for the gene microarray studies.

Supporting Online Material
www.sciencemag.org/cgi/content/full/310/5749/850/DC1
Materials and Methods
Figs. S1 to S5
Tables S1 to S5
References and Notes

19 July 2005; accepted 5 October 2005
10.1126/science.1117634

Regulated Pole-to-Pole Oscillations of a Bacterial Gliding Motility Protein

Tâm Mignot, John P. Merlie Jr., David R. Zusman*

Little is known about directed motility of bacteria that move by type IV pilus–mediated (twitching) motility. Here, we found that during periodic cell reversals of *Myxoccocus xanthus*, type IV pili were disassembled at one pole and reassembled at the other pole. Accompanying these reversals, FrzS, a protein required for directed motility, moved in an oscillatory pattern between the cell poles. The frequency of the oscillations was controlled by the Frz chemosensory system, which is essential for directed motility. Pole-to-pole migration of FrzS appeared to involve movement along a filament running the length of the cell. FrzS dynamics may thus regulate cell polarity during directed motility.

Gliding motility is important for bacterial movement on solid surfaces, virulence, and development (*1*). Twitching motility in *Pseudomonas aeruginosa* or social motility (S-motility) in *Myxococcus xanthus* involves assembly of type IV pili at the leading end of cells: Motion is produced as the fibers bind to receptors on the substratum, or another cell, and retract (*2*). Control of directional movements requires periodic cell reversals, which are regulated by chemosensory systems (*1*, *3*, *4*). It has been proposed that cellular reversals are achieved by switching the sites of pili extrusion from one cell pole to the other (*4*).

In *M. xanthus*, directed motility allows cells to coordinate movements toward nutrients or, when limiting, fruiting bodies (*5*). FrzS is required for S-motility–dependent vegetative swarming. It contains an N terminal receiver–like domain, an alanine-proline–rich linker, and an extended coiled-coil domain (fig. S1A) (*6*). *frzS* mutants are impaired in S-motility swarming because they are defective in regulating pili–mediated directional movements (fig. S1, B and C). Indeed, mutants that have strong directional defects cannot swarm or form fruiting bodies (*7*, *8*).

University of California, Department of Molecular and Cell Biology, Berkeley, CA 94720–3204, USA.

*To whom correspondence should be addressed. E-mail: zusman@uclink.berkeley.edu

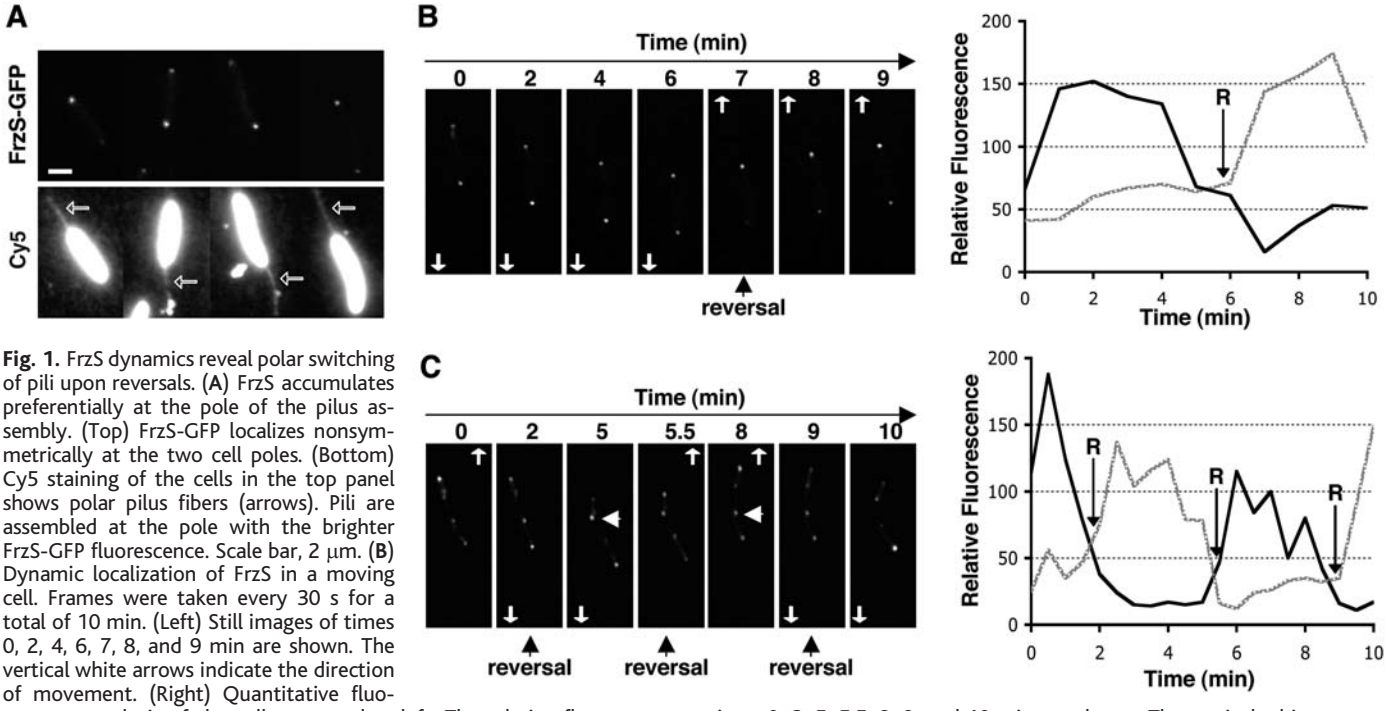

Fig. 1. FrzS dynamics reveal polar switching of pili upon reversals. (**A**) FrzS accumulates preferentially at the pole of the pilus assembly. (Top) FrzS-GFP localizes nonsymmetrically at the two cell poles. (Bottom) Cy5 staining of the cells in the top panel shows polar pilus fibers (arrows). Pili are assembled at the pole with the brighter FrzS-GFP fluorescence. Scale bar, 2 μm. (**B**) Dynamic localization of FrzS in a moving cell. Frames were taken every 30 s for a total of 10 min. (Left) Still images of times 0, 2, 4, 6, 7, 8, and 9 min are shown. The vertical white arrows indicate the direction of movement. (Right) Quantitative fluorescence analysis of the cell presented at left. The relative fluorescence intensities (arbitrary units) of each cell pole were measured and plotted over time. Black line, initial leading pole; gray line, initial trailing pole; R, Reversal. (**C**) Dynamic localization of FrzS in a *frzCD*^{c} mutant cell. Frames were taken every 30 s for a total duration of 10 min. (Left) Still images of times 0, 2, 5, 5.5, 8, 9, and 10 min are shown. The vertical white arrows indicate the direction of movement. Horizontal white arrows point to *frzCD*^{c} –dependent additional FrzS spots that brighten immediately before switch of the bright pole. (Right) Quantitative fluorescence analysis of the cell presented at left. Labels as in (B).